

1 **The Incredible Lightness of Water Vapor**

2 Da Yang* and Seth D. Seidel

3 *University of California, Davis*

4 *Lawrence Berkeley National Laboratory, Berkeley*

Submitted to Journal of Climate on April 4, 2019
Review received on June 20, 2019
Revision submitted on July 27, 2019

5 *Corresponding author address: Da Yang, 253 Hoagland Hall, Davis, CA 95616.

6 E-mail: dayang@ucdavis.edu

ABSTRACT

7 The molar mass of water vapor is much less than that of dry air. This makes
8 a moist parcel lighter than a dry parcel of the same temperature and pres-
9 sure. This effect is known as the vapor buoyancy effect and has often been
10 overlooked in climate studies. We propose that the vapor buoyancy effect
11 increases Earth's outgoing longwave radiation (OLR) and that this negative
12 radiative effect increases with warming, stabilizing Earth's climate. We illus-
13 trate this mechanism in an idealized tropical atmosphere, where there is no
14 horizontal buoyancy gradient in the free troposphere. Temperature increases
15 toward dry atmosphere columns to compensate reduction of vapor buoyancy,
16 increasing OLR by $O(1 \text{ W/m}^2)$ at the reference climate. In warmer climates,
17 the temperature difference between moist and dry columns would increase
18 due to increasing atmospheric water vapor, leading to enhanced radiative ef-
19 fect and thereby stabilizing Earth's climate. We estimate that this feedback
20 strength is about $O(0.2 \text{ W/m}^2/\text{K})$ in the idealized atmosphere, which com-
21 pares with cloud feedback and surface albedo feedback in the current climate.
22 We further show evidence from observations and real-gas radiative transfer
23 calculations for a significant radiative effect of vapor buoyancy in the tropical
24 atmosphere.

25 **1. Introduction**

26 How fast would Earth's climate respond to increasing CO₂ (Manabe and Wetherald 1975; Flato
27 et al. 2013; Collins et al. 2013)? Why is tropical climate more stable than extratropical climate
28 (Holland and Bitz 2003; Polyakov et al. 2002; Pierrehumbert 1995)? What sets the inner edge
29 of the habitable zone of Earth-like planets (Yang and Abbot 2014; Pierrehumbert 2010)? Under-
30 standing and accurately estimating climate feedbacks are key to address these pressing questions.

31 The importance of water vapor seems to be widely recognized in the literature of climate feed-
32 backs (Manabe and Wetherald 1967; Ingersoll 1969; Held and Soden 2000; Flato et al. 2013).
33 Previous studies have focused on three basic effects of water vapor: E1) water vapor is a green-
34 house gas; E2) water vapor can condense to liquid water and release latent heat; E3) saturation
35 vapor pressure increases with temperature exponentially. The combination of E1 and E3 gives rise
36 to the water vapor feedback, the dominant positive climate feedback (Manabe and Wetherald 1967;
37 Held and Soden 2000; Flato et al. 2013). Increasing temperature leads to more water vapor, which
38 leads to an enhanced greenhouse effect, warming the planet further. The water vapor feedback
39 could even lead to a runaway greenhouse state when the atmosphere is sufficiently opaque to long-
40 wave radiation that the outgoing longwave radiation (OLR) is insensitive to surface temperature
41 (Ingersoll 1969). The combination of E2 and E3 gives rise to the (tropical) lapse rate feedback, a
42 negative climate feedback in the tropical atmosphere (Flato et al. 2013). Increasing temperature
43 leads to more water vapor, which leads to less steep lapse rate in the tropical atmosphere. This
44 effect increases upper troposphere temperature more than the lower troposphere, leading to higher
45 emission of outgoing longwave radiation (OLR), which cools the planet. At higher latitudes, tem-
46 perature lapse rate is no longer controlled by moist convection, so the lapse rate feedback is less
47 constrained. Both feedbacks are among the five most important climate feedbacks in the Intergov-

48 ernmental Panel on Climate Change (IPCC) reports and have been extensively evaluated in general
49 circulation models (GCMs) (Flato et al. 2013).

50 However, the lightness of water vapor has been completely overlooked in the context of climate
51 feedbacks. In Earth’s atmosphere, buoyancy is represented by the virtual temperature [*e.g.*, see (5)
52 in Yang (2018a)]. We define the virtual temperature

$$T_v = T \left(\frac{1 + r/\varepsilon}{1 + r} \right), \quad (1)$$

53 where T is temperature, r is water vapor mixing ratio, and $\varepsilon = M_v/M_d$. The molar mass of water
54 vapor M_v is 18 g/mol, significantly lighter than that of dry air M_d , which is 29 g/mol. This makes a
55 moist parcel lighter than a dry parcel of the same temperature and pressure (Emanuel 1994). Here
56 we refer to this as the vapor buoyancy effect, though it is also referred to as the virtual effect (Yang
57 2018a,b). The vapor buoyancy effect makes T_v slightly higher than T by $O(1 \text{ K})$ in the tropical
58 atmosphere, which is of the same order of magnitude as typical temperature fluctuations there.

59 We propose that the vapor buoyancy effect can increase Earth’s OLR and helps stabilize Earth’s
60 climate by regulating the atmosphere’s thermal structure. Figure 1 shows temperature and virtual
61 temperature (buoyancy) fields in the moisture space from 2°S to 2°N using NASA AIRS data. In
62 the free troposphere ($p < 850 \text{ hPa}$), buoyancy is horizontally uniform because of the small Coriolis
63 parameter and efficient gravity waves (Charney 1963; Bretherton and Smolarkiewicz 1989; Sobel
64 et al. 2001; Yang 2018a). However, temperature increases toward dry columns due to the vapor
65 buoyancy effect. Moving toward the dry columns, moisture and its associated vapor buoyancy
66 are reduced. To maintain uniform buoyancy, temperature has to increase. We propose that the
67 temperature tilt would increase with climate warming due to increasing atmospheric moisture,
68 leading to enhanced OLR over the dry area. This is a negative feedback and can stabilize Earth’s
69 climate.

70 Previous studies implied that vapor buoyancy could make temperature increase toward dry
71 columns in the tropical atmosphere (Tompkins 2001; Bretherton and Smolarkiewicz 1989;
72 Bretherton et al. 2005; Yang 2018b,a). However, they have often considered this effect to be
73 small and negligible, simplifying the dynamics according to a weak temperature gradient approx-
74 imation (Sobel et al. 2001). These studies, therefore, did not consider that its radiative effect is
75 significant, which is the novelty of this study.

76 In Section 2, we explain our hypothesis in detail. We first illustrate how the vapor buoyancy ef-
77 fect increases Earth’s OLR (a negative radiative effect) and then explain why this effect strengthens
78 with climate warming. In Section 3, we derive a simple model for the radiative effect and feedback
79 strength of the vapor buoyancy effect. We then use the simple model to make order-of-magnitude
80 estimates for the radiative effect and feedback strength. In Section 4, we estimate the radiative
81 effect by using tropical sounding profiles with a real-gas radiative transfer model. In Section 5, we
82 conclude and discuss implications on the climate stability of Earth and other planets.

83 **2. Hypothesis**

84 We propose that the vapor buoyancy can increase OLR (a negative radiative effect) due to a clear-
85 sky effect, and that the radiative effect increases with climate warming. Figure 2 illustrates our
86 hypothesis by comparing OLR from two stand-alone atmospheres with overturning circulations:
87 one considers the vapor buoyancy effect (control), the other does not consider this effect. The
88 overturning circulation is analogous to the Walker Circulation or convective self-aggregation in
89 the tropics (Bretherton et al. 2005; Pritchard and Yang 2016; Yang and Ingersoll 2013, 2014).
90 The upwelling branch of the circulation is associated with deep convection and moist air, and the
91 downwelling branch is associated with clear sky and dry air. For illustrative purposes, we make a
92 few simplifications: S1) the two atmospheres are non-rotating; S2) the two atmospheres sit above

93 ocean surface with the same, uniform surface temperature; S3) the two atmospheres have the
94 same water vapor distribution. The first two simplifications are relevant to the tropical atmosphere
95 as the rotation effect and surface temperature gradient are both weak in the tropics. The third
96 simplification is often required when calculating the radiative effect.

97 Figure 2 shows that the control atmosphere emits more OLR than the no-vapor-buoyancy atmo-
98 sphere due to higher temperature in the dry area. OLR is primarily a function of temperature and
99 water vapor mixing ratio r . When r remains the same in the two atmospheres (S3), the OLR dif-
100 ference would come from temperature differences between the two atmospheres. Here we provide
101 physical intuition on why there should be temperature differences, leaving detailed derivation in
102 Section 3e. The temperature profiles of moist areas in the two atmospheres are set by convective
103 plumes. Because these convective plumes rise from the same surface temperature, the temperature
104 profiles should be almost identical in the two moist areas. Temperature profiles in the dry areas,
105 however, differ significantly, leading to differences in OLR. According to long-accepted results in
106 geophysical fluid dynamics, the horizontal buoyancy gradient is negligible in the free troposphere
107 without rotation because gravity waves can effectively smooth out buoyancy anomalies (Charney
108 1963; Sobel et al. 2001). We refer to this effect as the weak buoyancy gradient (WBG) approxi-
109 mation (Yang 2018a). In the control atmosphere, buoyancy is a function of both temperature and
110 and water vapor mixing ratio r due to the vapor buoyancy effect. The horizontal moisture gradient
111 then leads to horizontal temperature gradient: dry air is warmer than moist air. In the no-vapor-
112 buoyancy atmosphere, temperature is uniformly distributed in the free troposphere, as buoyancy
113 is a function of temperature only. The dry column of the control atmosphere, therefore, is warmer
114 than that of the no-vapor-buoyancy atmosphere by $O(1 \text{ K})$, leading to enhanced OLR. The spectra
115 of H_2O in the longwave is also sensitive to temperature. However, this impact is likely small.

116 In warmer climates, the vapor buoyancy effect would become more significant due to increasing
117 water vapor. Therefore, we expect that the radiative effect due to the vapor buoyancy also increases
118 with climate warming. This is a negative climate feedback (Fig. 2b). The proposed mechanism
119 relies on ample atmospheric water vapor, so it would be most effective in stabilizing the tropical
120 climate. In principal, this feedback should have been represented by climate models. However, it
121 has not been evaluated nor even discussed.

122 We will construct a simple model of the proposed feedback mechanism. This will give an order-
123 of-magnitude estimate of the associated radiative effect and the rate at which it increases with
124 climate warming.

125 **3. A simple model**

126 We construct a simple model based on the schematic diagram (Fig. 2). Each atmosphere with
127 overturning circulations is represented by a dry column and a moist column (Pierrehumbert 1995).
128 Because the moist columns would have the same temperature profiles, the OLR difference pri-
129 marily comes from the dry columns, which we will focus on. Again, we aim to estimate the
130 "radiative effect" due to the vapor buoyancy effect. Therefore, we assume that all basic dynamic
131 (*e.g.*, circulation and pressure) and thermodynamic features (*e.g.*, moisture) are the same in the
132 two atmospheres—one with the vapor buoyancy effect, and the other without it.

133 The goal of this simple model is to provide an order-of-magnitude understanding of our hypoth-
134 esis. Therefore, we employ a two-band radiative transfer model. The two-band model is more
135 realistic than a gray atmosphere model by allowing two absorption bands with distinct absorption
136 coefficients, leading to different emission levels. The two band model is, on the other hand, much
137 simpler than a real-gas radiative transfer model, so the results are easier to interpret.

138 *a. The two-band model*

139 We consider a plane-parallel atmosphere. Only the clear-sky longwave (IR) radiation is con-
 140 sidered, and the IR opacity is mainly due to water vapor. Here we parameterize the water vapor
 141 absorption spectrum by two broad bands that occupy roughly equal fractions of blackbody emis-
 142 sion at Earth-like temperatures (Beucler and Cronin 2016): one with a strong absorption coefficient
 143 (κ_S) and the other with a weak absorption coefficient (κ_W).

144 We first consider one absorption band with any given κ . OLR is defined as

$$OLR^\kappa \equiv F^\uparrow(p=0) - F^\downarrow(p=0), \quad (2)$$

145 where F^\uparrow and F^\downarrow are upward and downward longwave radiative fluxes. We know that $F^\downarrow(0) \approx 0$,
 146 so a primary focus is to solve for $F^\uparrow(0)$ in the gray atmosphere, which is given by

$$\frac{dF^\uparrow}{d\tau} = F^\uparrow - \sigma T^4, \quad (3)$$

147 where T is temperature, τ is optical depth, and σ is the Stefan-Boltzmann constant. We integrate
 148 (3) and get

$$F^\uparrow(0) = e^{-\tau_s} F^\uparrow(\tau_s) + \int_0^{\tau_s} \sigma T^4 \times e^{-\tau'} d\tau'. \quad (4)$$

149 The OLR is then given by

$$OLR^\kappa = e^{-\tau_s} \sigma T_s^4 + \int_0^{\tau_s} \sigma T^4 \times e^{-\tau'} d\tau', \quad (5)$$

150 where A_s represents the surface value of A , and we have used $F^\uparrow(\tau_s) = \sigma T_s^4$. This equation shows
 151 that OLR has two components: one is the surface contribution, and the other is the atmosphere
 152 contribution.

153 We now use (5) to calculate the OLR difference between the two atmospheres, each containing
 154 one moist and one dry columns. We remind the readers that T_s , r and thereby τ of the two atmo-
 155 spheres are identical, so the OLR difference primarily comes from dry columns, in which there is

156 significant air temperature difference. The OLR difference of the dry column is given by

$$\Delta OLR^K \equiv OLR_v^K - OLR_{nv}^K \approx \int_0^{\tau_s} 4\sigma T_d^3 \Delta T \times e^{-\tau'} d\tau' \approx \int_0^{\tau_s} 4\sigma T_m^3 \Delta T \times e^{-\tau'} d\tau', \quad (6)$$

157 where OLR_v and OLR_{nv} represent OLR in the atmosphere with and without the vapor buoyancy
 158 effect. In the last equal sign, we assumed that $(T_d - T_m)/T_m \ll 1$. Because the strong and weak
 159 absorption bands occupy equal portions of the spectrum, the total OLR difference is given by

$$\Delta OLR = 0.5 \times (\Delta OLR^{Ks} + \Delta OLR^{Kw}). \quad (7)$$

160 To compute ΔOLR , we need information of T_m , ΔT , τ , and thereby r , which is the mixing ratio of
 161 water vapor.

162 *b. Temperature*

163 In the Earth's tropical atmosphere, temperature profiles can be approximated by power-law re-
 164 lations of pressure:

$$T = T_s \left(\frac{p}{p_s} \right)^{R_d \Gamma_M / g}, \quad (8)$$

165 where T_s is the surface temperature, p_s is surface pressure, R_d is the gas constant for dry air,
 166 Γ_M is the moist adiabatic lapse rate, and g is gravity acceleration. This has been referred to as
 167 the "all-troposphere model" by Pierrehumbert (2010), as the lapse rate is entirely determined by
 168 moist convection. Equation (8) fits the observed temperature profiles in the tropical troposphere,
 169 but introduces significant biases in the stratosphere (Beucler and Cronin 2016). Earth's OLR is
 170 dominated by tropospheric contributions, which justifies the use of (8).

171 *c. Moisture*

172 The water vapor mixing ratio r is the ratio of the mass of water vapor to the mass of dry air and
173 is given by

$$r = RH \times r^*(T, p), \quad (9)$$

174 where RH is the relative humidity, and r^* is the saturation mixing ratio. For the moist column, we
175 assume that $r_m = r_m^*$ ($RH = 1$) at all vertical levels; For the dry column, we have $r = \beta \cdot r_m^*$, where
176 $0 < \beta < 1$. Here β is a more convenient parameter than the relative humidity of dry columns (RH_d).
177 This is because, at given T_s , the two dry columns are of different temperatures, so they would have
178 different RH values corresponding to same mixing ratio. In reality, β could have complicated
179 vertical structures, which requires multiple parameters to describe. For the purpose of illustrating
180 the proposed mechanism with minimal parameters, we take β as a constant at all vertical levels.
181 This simplification may affect the results quantitatively but will not affect the results qualitatively.

182 *d. Optical depth*

183 Outgoing longwave radiation is observed from space, so it would be convenient to define the
184 optical depth τ as an increasing function as pressure. We thus require that $\tau(p = 0) = 0$. We write
185 the optical depth as

$$d\tau = \kappa \cdot r \cdot \frac{dp}{g}. \quad (10)$$

186 The optical depth would have different values for the two absorption bands: $d\tau = \kappa^s \cdot r \cdot dp/g$ for
187 the strong band, and $d\tau = \kappa^w \cdot r \cdot dp/g$ for the weak band. In this model, we ignore the pressure-
188 broadening effect and treat the absorption coefficients as constant: $\kappa^s = 1.66 \times 0.1$ (m^2/kg) and
189 $\kappa^w = 1.66 \times 0.02$ (m^2/kg), where the factor of 1.66 is referred to as the diffusivity factor (Pier-
190 rehumbert 2010). Here the absorption coefficients are consistent with previous modeling studies

191 of similiar complexity (Ingersoll 1969; Pierrehumbert 2010; Beucler and Cronin 2016). We can
 192 integrate (10) to obtain the optical depth at an arbitrary pressure level

$$\tau(p) = \int_0^p \kappa \cdot r \cdot \frac{dp'}{g}. \quad (11)$$

193 At surface $p = p_s$, we then have $\tau_s \equiv \tau(p_s) = \int_0^{p_s} \kappa \cdot r \cdot dp'/g$. Here τ_s measures the optical depth
 194 at the surface, which is total optical depth of the atmospheric column.

195 *e. The WBG approximation and ΔT*

196 Buoyancy is horizontally homogenized in the tropical free troposphere (Fig. 1). We refer to
 197 this constraint as the weak buoyancy gradient (WBG) approximation (Yang 2018a). This is an
 198 improvement of the weak temperature gradient (WTG) approximation, which neglects the vapor
 199 buoyancy effect (Charney 1963; Sobel et al. 2001). In a moist atmosphere, buoyancy is related to
 200 the virtual temperature, which is given by

$$T_v = T \left(\frac{1 + r/\varepsilon}{1 + r} \right), \quad (12)$$

201 where $\varepsilon = M_v/M_d$, where M_v and M_d represent the molar mass of water vapor and dry air, respec-
 202 tively. In the free troposphere, uniform buoyancy requires the virtual temperature to be uniform
 203 across the moist and dry area:

$$T_m \left(\frac{1 + r_m/\varepsilon}{1 + r_m} \right) = T_d \left(\frac{1 + r_d/\varepsilon}{1 + r_d} \right). \quad (13)$$

204 We substitute $T_d = T_m + \Delta T_{WBG}$ into (13) and get

$$\Delta T_{WBG} = T_m \left(\frac{1 + r_m/\varepsilon}{1 + r_m} - \frac{1 + r_d/\varepsilon}{1 + r_d} \right) \left(\frac{1 + r_d}{1 + r_d/\varepsilon} \right). \quad (14)$$

205 Equation (14) is derived without approximations about the amount of water vapor and the ampli-
 206 tude of ΔT . Although this form is quite accurate, we would like to simplify it by assuming water

207 vapor is a trace gas: $r \ll 1$. This is a good assumption for the current climate and may still be
 208 good till surface temperature reaches 320 K, at which temperature $r^*(p_s) = 73$ g/kg. With this
 209 approximation, we get

$$\Delta T_{WBG} = T_m \left(\frac{1}{\epsilon} - 1 \right) (r_m - r_d). \quad (15)$$

210 This simplified equation clearly tells that ΔT depends on the contrast, not just absolute values, of
 211 mixing ratio and molar mass.

212 The above calculation is more accurate in the free troposphere, where gravity waves efficiently
 213 smooth out buoyancy anomalies. Although there is no such constraints in the boundary layer, we
 214 can assume that $\Delta T = 0$ at the surface temperature because of the uniform sea surface temperature
 215 (SST). We, therefore, require ΔT equals ΔT_{WBG} in the free troposphere but smoothly decays to 0
 216 at surface:

$$\Delta T = \Delta T_{WBG} \times \left[1 - \left(\frac{p}{p_s} \right)^n \right], \quad (16)$$

217 where n controls the decay rate with pressure. The p/p_s term would decay faster (slower) with
 218 large (small) n , so different n could potentially result in different amplitudes and altitudes of the
 219 maximum temperature difference. We, however, find that the values of ΔOLR and its sensitivity
 220 to surface temperature only change by 50% while we vary n over an order of magnitude, from
 221 5 to 50. Therefore, we conclude the results are robust to the choice of n , and we take $n = 30$ in
 222 the following calculation. Figure 3a shows ΔT profiles with different β values at different surface
 223 temperatures: ΔT decreases with β and increases with T_s . At 300 K surface temperature, the
 224 maximum of ΔT is about 0.45 K when $\beta = 0.8$; the maximum of ΔT is about 1.1 K when $\beta = 0.5$;
 225 the maximum of ΔT is about 1.7 K when $\beta = 0.2$. We find that ΔT increases faster with T_s in
 226 drier columns, which would be used to explain the sensitivity of ΔOLR to T_s .

227 Equations (6-10, 16) form the complete set of this model. With proper parameter values, we can
 228 estimate the magnitude of ΔOLR and its change with surface temperature.

229 *f. Results*

230 Our calculation shows that the vapor buoyancy effect can significantly impact Earth's energy
 231 balance and future climate changes. Figure 4a shows that ΔOLR is of $O(4 \text{ W/m}^2)$ for a wide range
 232 of parameter values. In the reference climate ($T_s = 300 \text{ K}$), ΔOLR is about 2.5 W/m^2 with $\beta = 0.5$,
 233 a similar magnitude to the radiative effect due to doubling CO_2 . We then understand the sensitivity
 234 of ΔOLR to T_s and β according to (6).

- 235 • ΔOLR increases with T_s at given β . This is mainly because ΔT increase with warming, as
 236 will be quantified in Figs. 4b & 4c.
- 237 • ΔOLR is small at both moist and dry limits. In the moist limit ($\beta \rightarrow 1$), ΔT is small according
 238 to (15). In the dry limit ($\beta \rightarrow 0$), although ΔT maximizes, ΔOLR is dominated by surface
 239 emission, insensitive to ΔT . The OLR difference, therefore, peaks at intermediate β values.
- 240 • The ΔOLR peak shifts toward smaller β in warmer climates. This is because, at high temper-
 241 atures, ΔT increases faster with warming in the small- β columns (Fig. 3a) and also because
 242 the large- β columns become increasingly opaque to IR emission (Fig. 3b-c).

243 Consistent with our hypothesis, ΔOLR increases with T_s , showing a negative climate feedback.

244 To quantify the feedback strength, we define feedback parameters

$$\lambda_t = \frac{d\Delta OLR}{dT_s}, \quad (17)$$

$$\lambda_{vb} = \left. \frac{d\Delta OLR}{dT_s} \right|_{T, \tau}, \quad (18)$$

246 where λ_t is the total sensitivity of ΔOLR to T_s , and λ_{vb} is the vapor-buoyancy feedback parameter,
 247 which only concerns $d\Delta T/dT_s$. Figure 4b shows that λ_t is of $O(0.2 \text{ W/m}^2/\text{K})$ in the reference

248 climate, which compares with the feedback strength due to clouds and surface albedo. The feed-
249 back parameter keeps increasing with surface temperature and reaches about $1.4 \text{ W/m}^2/\text{K}$ at 320
250 K, suggesting that the vapor buoyancy effect becomes increasingly important in future climates.

251 Figure 4c shows that λ_{vb} is of similar magnitude to λ_t , suggesting the vapor-buoyancy feedback
252 dominates the entire ΔOLR sensitivity to T_s . We find that λ_{vb} is small at the moist and dry limits.
253 This is because $\Delta T \rightarrow 0$ when $\beta \rightarrow 1$ at all surface temperatures, and ΔOLR is dominated by
254 surface emission when $\beta \rightarrow 0$ at all surface temperatures, not feeling ΔT and its changes. In
255 addition, we find that the peak of λ_{vb} moves towards small- β columns with warming because ΔT
256 increases faster with warming at small- β columns (Fig. 3a), and also because large- β columns
257 become increasingly opaque at high temperature (Fig. 3b-c), insensitive to changes of ΔT that
258 peaks in the lower troposphere.

259 The overall results do not depend on the assumed ΔT profiles in the boundary layer. Figure
260 4d-f shows ΔOLR , λ_t , and λ_{vb} for the free troposphere ($p < 900 \text{ hPa}$). The free-troposphere results
261 almost reproduce the full-column results, with amplitudes of 10 - 15% weaker than the full-column
262 calculation. This suggests that the vapor-buoyancy radiative effect and feedbacks occur primarily
263 in the free troposphere.

264 **4. Observation: A case study**

265 We estimate the radiative effect due to the vapor buoyancy using *in-situ* observed temperature
266 and moisture profiles from the Nauru Atmospheric Radiation Measurement (ARM) site during the
267 period from April 2001 to August 2013 (Fig. 5). The method of this calculation is based on the
268 two column model developed in Fig. 2 and in Section 3. We assume that, in the free troposphere,
269 buoyancy of this atmospheric column is the same as that of a saturated, convecting atmospheric
270 column, and then we solve for the temperature profile of the convecting column using (13). This

271 derived temperature profile corresponds to that of an atmosphere without the vapor buoyancy effect
272 (Fig. 2a) and is about 0.8 K colder than the observed temperature profile in the lower troposphere
273 (Fig. 5d).

274 We then compute the clear-sky OLR of the two columns by using the Rapid Radiative Transfer
275 Model [RRTM v3.3, Mlawer et al. (1997)]. The model was run using 28 vertical levels between
276 1013 hPa to 55 hPa. The CO₂ mixing ratio is set at 400ppm, and all other trace gases, including
277 ozone, were set to zero. The clear-sky OLR of the observed atmospheric column is 300.4 (W/m²);
278 the clear-sky OLR of the no-vapor-buoyancy column is 299.3 (W/m²). Therefore, the vapor buoy-
279 ancy effect is responsible for about 1.1 W/m² increase in clear-sky OLR for a typical atmospheric
280 column in the deep tropics. This result is encouraging as it agrees well with our simple model
281 calculations at 300 K surface temperature. If we shift the boundary layer top from 900 hPa to
282 800 hPa, this OLR difference would be 0.9 W/m², which remains significant. This sensitivity test
283 suggests that the radiative effect of vapor buoyancy primarily originates from the free troposphere.

284 This case study is a first step toward quantifying the radiative effect of vapor buoyancy in Earth's
285 atmosphere. Future analyses should expand this study by using global-scale data sets, providing
286 a more accurate estimate of the radiative effect of vapor buoyancy over the entire tropical atmo-
287 sphere.

288 **5. Conclusion and discussion**

289 The conventional wisdom is that the vapor buoyancy effect is small, so its impact on temperature
290 is negligible in the free troposphere. However, using NASA AIRS observations, we have demon-
291 strated that the vapor buoyancy effect could lead to about 1.5 K horizontal temperature difference
292 in the lower troposphere from the driest column to the moistest column (Fig. 1), which has a
293 significant impact on Earth's radiative balance.

294 Based on the novel observation, this paper proposes that the vapor buoyancy effect can increase
295 Earth's OLR by increasing the air temperature in the dry columns. We have developed a simple
296 model that computes the OLR difference between two atmospheres: one with the vapor buoyancy
297 effect, and the other without this effect. We show that the magnitude of this effect is of $O(1$
298 $\text{W/m}^2)$ at $T_s = 300 \text{ K}$, which is then confirmed by observations, and that it increases rapidly with
299 climate warming due to an exponential increase of atmospheric water vapor, leading to a negative
300 climate feedback (Fig. 2b). We further show that the feedback strength λ is of $O(0.2 \text{ W/m}^2/\text{K})$, the
301 amplitude of which compares with major climate feedback, including cloud feedback and surface
302 albedo feedback. Therefore, faithful representation of the vapor buoyancy effect in climate models
303 is necessary for accurate estimates of climate sensitivity and reliable predictions for future climate
304 changes.

305 The vapor buoyancy effect may help explain why tropical climate has been more stable than
306 extratropical climate (Holland and Bitz 2003; Polyakov et al. 2002; Pierrehumbert 1995). The
307 strength of the vapor buoyancy feedback depends on water vapor contrast between moist and
308 dry columns, which in turn depends on water vapor abundance and thereby temperature of the
309 atmosphere. This effect, therefore, operates more efficiently in the tropics and less efficiently at
310 higher latitudes. This spatial pattern may explain why fluctuations of sea surface temperature in the
311 tropics are much smaller than that of higher latitudes in the past 100 million years (Pierrehumbert
312 1995).

313 The vapor buoyancy effect helps extend the inner edge of the habitable zone, in particular, for
314 tidally locked exoplanets. Tidally locked planets are often slowly rotating, so their free troposphere
315 could be in the WBG regime globally (Koll and Abbot 2016; Mills and Abbot 2013). These plan-
316 ets have one fixed diurnal hemisphere and one nocturnal hemisphere, corresponding to the moist
317 and dry columns of our model, respectively. When the tidally locked planets are approaching

318 the inner edge of the habitable zone, their surface temperature could be significantly higher than
319 Earth’s tropical SST, providing an ideal environment for the vapor buoyancy feedback to work ef-
320 ficiently. However, previous studies have neglected the vapor buoyancy effect and assumed WTG
321 (Yang et al. 2013; Yang and Abbot 2014; Pierrehumbert 2010), which could lead to considerably
322 narrower habitable zones. Therefore, we suggest that the vapor buoyancy effect should be accu-
323 rately represented not only in GCMs but also in low-order models that are used to study climate
324 habitability.

325 To focus on order-of-magnitude understanding, we have inevitably introduced simplifications to
326 our model that only considers the clear-sky longwave radiation. An important one is that we use
327 the two-band radiative transfer model, lacking detailed representation of water vapor’s absorption
328 spectrum. We have also assumed that β is uniform in altitude, whereas β often has complicated
329 vertical structures in the real atmosphere. However, a suite of cloud-resolving model (CRM) sim-
330 ulations has shown similar estimates of ΔOLR and λ . The CRM uses a comprehensive radiation
331 scheme and explicitly simulates atmospheric circulation and water vapor dynamics. The CRM
332 results have also shown that the vapor buoyancy effect does not affect the short-wave radiation
333 budget and that the clear-sky effect dominates the OLR response. The CRM results, therefore,
334 justify our simplifications and will be presented in a companion paper (Seidel and Yang 2018).

335 *Acknowledgments.* This work was supported by Laboratory Directed Research and Development
336 (LDRD) funding from Berkeley Lab, provided by the Director, Office of Science, of the U.S.
337 Department of Energy under contract DE-AC02-05CH11231 and used resources of the National
338 Energy Research Scientific Computing Center (NERSC), also supported by the Office of Science
339 of the U.S. Department of Energy, under Contract no. DE-AC02-05CH11231. The authors thank
340 Dr. Z. Tan and two anonymous reviewers for helpful comments and suggestions.

341 **References**

- 342 Beucler, T., and T. W. Cronin, 2016: Moisture-radiative cooling instability. URL <http://doi.wiley.com/10.1002/2016MS000763>, 1620–1640 pp., doi:10.1002/2016MS000763.
- 343
- 344 Bretherton, C. S., P. N. Blossey, and M. Khairoutdinov, 2005: An Energy-Balance Analysis of
345 Deep Convective Self-Aggregation above Uniform SST. *Journal of the Atmospheric Sciences*,
346 **62 (12)**, 4273–4292, doi:10.1175/JAS3614.1.
- 347 Bretherton, C. S., and P. K. Smolarkiewicz, 1989: Gravity waves, compensating subsidence and
348 detrainment around cumulus clouds. *Journal of the Atmospheric Sciences*, **46 (6)**, 740–759,
349 doi:10.1175/1520-0469(1989)046<0740:GWCSAD>2.0.CO;2.
- 350 Charney, J. G., 1963: A Note on Large-Scale Motions in the Tropics. *Journal of the Atmo-*
351 *spheric Sciences*, **20 (6)**, 607–609, doi:10.1175/1520-0469(1963)020<0607:ANOLSM>2.0.CO;
352 2, URL [http://journals.ametsoc.org/doi/abs/10.1175/1520-0469{\%}281963{\%}29020{\%}](http://journals.ametsoc.org/doi/abs/10.1175/1520-0469%7B%7D281963%7B%7D29020%7B%7D3C0607%7B%7D3AANOLSM%7B%7D3E2.0.CO%7B%7D3B2)
353 [}3C0607{\%}3AANOLSM{\%}3E2.0.CO{\%}3B2](http://journals.ametsoc.org/doi/abs/10.1175/1520-0469%7B%7D281963%7B%7D29020%7B%7D3C0607%7B%7D3AANOLSM%7B%7D3E2.0.CO%7B%7D3B2).
- 354 Collins, M., and Coauthors, 2013: Long-term Climate Change: Projections, Commitments and
355 Irreversibility. In: *Climate Change 2013: The Physical Science Basis. Contribution of Working*
356 *Group I to the Fifth Assessment Report of the Intergovernmental Panel on Climate Change*
357 *[Stocker, T.F., D. Qin, G.-K. Plattner, M. Tignor, S.K. Allen, J. Boschung, A. Nauels, Y. Xia, V.*
358 *Bex and P.M. Midgley (eds.)]. Cambridge University Press, Cambridge, United Kingdom and*
359 *New York, NY, USA.*
- 360 Emanuel, K. A., 1994: *Atmospheric convection*. Oxford University press. 1994. pp. 580. isbn 0
361 19 5 6630 8.

362 Flato, G., and Coauthors, 2013: Evaluation of Climate Models. In: Climate Change 2013:
363 The Physical Science Basis. Contribution of Working Group I to the Fifth Assessment Re-
364 port of the Intergovernmental Panel on Climate Change [Stocker, T.F., D. Qin, G.-K. Plattner,
365 M. Tignor, S.K. Allen, J. Boschung, A. Nauels, Y. Xia, V. Bex and P.M. Midgley (eds.)].
366 Cambridge University Press, Cambridge, United Kingdom and New York, NY, USA. doi:
367 10.1017/CBO9781107415324.020.

368 Held, I. M., and B. J. Soden, 2000: Water vapor feedback and global warming. *Annual Review*
369 *of Energy and the Environment*, **25** (1), 441–475, doi:10.1146/annurev.energy.25.1.441, URL
370 <https://doi.org/10.1146/annurev.energy.25.1.441>.

371 Holland, M. M., and C. M. Bitz, 2003: Polar amplification of climate change in coupled models.
372 *Climate Dynamics*, **21** (3), 221–232, doi:10.1007/s00382-003-0332-6, URL [https://doi.org/10.](https://doi.org/10.1007/s00382-003-0332-6)
373 [1007/s00382-003-0332-6](https://doi.org/10.1007/s00382-003-0332-6).

374 Ingersoll, A. P., 1969: The runaway greenhouse: A history of water on venus. *Journal of the*
375 *Atmospheric Sciences*, **26** (6), 1191–1198, doi:10.1175/1520-0469(1969)026<1191:TRGAHO>
376 2.0.CO;2, URL [https://doi.org/10.1175/1520-0469\(1969\)026<1191:TRGAHO>2.0.CO;2](https://doi.org/10.1175/1520-0469(1969)026<1191:TRGAHO>2.0.CO;2), [https://doi.org/10.1175/1520-0469\(1969\)026<1191:TRGAHO>2.0.CO;2](https://doi.org/10.1175/1520-0469(1969)026<1191:TRGAHO>2.0.CO;2).

378 Koll, D. D. B., and D. S. Abbot, 2016: TEMPERATURE STRUCTURE AND ATMOSPHERIC
379 CIRCULATION OF DRY TIDALLY LOCKED ROCKY EXOPLANETS. *The Astrophys-*
380 *ical Journal*, **825** (2), 99, doi:10.3847/0004-637x/825/2/99, URL [https://doi.org/10.3847/](https://doi.org/10.3847/0004-637x/825/2/99)
381 [0004-637x/825/2/99](https://doi.org/10.3847/0004-637x/825/2/99).

382 Manabe, S., and R. T. Wetherald, 1967: Thermal equilibrium of the atmosphere with
383 a given distribution of relative humidity. *Journal of the Atmospheric Sciences*, **24** (3),

384 241–259, doi:10.1175/1520-0469(1967)024<0241:TEOTAW>2.0.CO;2, URL [https://doi.org/](https://doi.org/10.1175/1520-0469(1967)024<0241:TEOTAW>2.0.CO;2)
385 10.1175/1520-0469(1967)024<0241:TEOTAW>2.0.CO;2.

386 Manabe, S., and R. T. Wetherald, 1975: The effects of doubling the co₂ concentration on
387 the climate of a general circulation model. *Journal of the Atmospheric Sciences*, **32** (1), 3–
388 15, doi:10.1175/1520-0469(1975)032<0003:TEODTC>2.0.CO;2, URL [https://doi.org/10.1175/](https://doi.org/10.1175/1520-0469(1975)032<0003:TEODTC>2.0.CO;2)
389 1520-0469(1975)032<0003:TEODTC>2.0.CO;2.

390 Mills, S. M., and D. S. Abbot, 2013: UTILITY OF THE WEAK TEMPERATURE GRADIENT
391 APPROXIMATION FOR EARTH-LIKE TIDALLY LOCKED EXOPLANETS. *The Astrophys-*
392 *ical Journal*, **774** (2), L17, doi:10.1088/2041-8205/774/2/L17, URL [https://doi.org/10.1088/](https://doi.org/10.1088/2041-8205/774/2/L17)
393 2041-8205/774/2/L17.

394 Mlawer, E. J., S. J. Taubman, P. D. Brown, M. J. Iacono, and S. A. Clough, 1997: Radiative
395 transfer for inhomogeneous atmospheres: Rrtm, a validated correlated-k model for the long-
396 wave. *Journal of Geophysical Research: Atmospheres*, **102** (D14), 16 663–16 682, doi:10.1029/
397 97JD00237, URL <https://agupubs.onlinelibrary.wiley.com/doi/abs/10.1029/97JD00237>.

398 Pierrehumbert, R. T., 1995: Thermostats, radiator fins, and the local runaway greenhouse. *Journal*
399 *of the Atmospheric Sciences*, **52** (10), 1784–1806, doi:10.1175/1520-0469(1995)052<1784:
400 TRFATL>2.0.CO;2, URL [https://doi.org/10.1175/1520-0469\(1995\)052<1784:TRFATL>2.0.](https://doi.org/10.1175/1520-0469(1995)052<1784:TRFATL>2.0.CO;2)
401 CO;2, [https://doi.org/10.1175/1520-0469\(1995\)052<1784:TRFATL>2.0.CO;2](https://doi.org/10.1175/1520-0469(1995)052<1784:TRFATL>2.0.CO;2).

402 Pierrehumbert, R. T., 2010: A PALETTE OF CLIMATES FOR GLIESE 581g. *The Astro-*
403 *physical Journal*, **726** (1), L8, doi:10.1088/2041-8205/726/1/L8, URL [https://doi.org/10.1088/](https://doi.org/10.1088/2041-8205/726/1/L8)
404 2041-8205/726/1/L8.

405 Pierrehumbert, R. T., 2010: *Principles of Planetary Climate*.

406 Polyakov, I. V., and Coauthors, 2002: Observationally based assessment of polar am-
407 plification of global warming. *Geophysical Research Letters*, **29** (18), 25–1–25–4,
408 doi:10.1029/2001GL011111, URL [https://agupubs.onlinelibrary.wiley.com/doi/abs/10.1029/](https://agupubs.onlinelibrary.wiley.com/doi/abs/10.1029/2001GL011111)
409 [2001GL011111](https://agupubs.onlinelibrary.wiley.com/doi/pdf/10.1029/2001GL011111), <https://agupubs.onlinelibrary.wiley.com/doi/pdf/10.1029/2001GL011111>.

410 Pritchard, M. S., and D. Yang, 2016: Response of the superparameterized Madden-Julian Oscil-
411 lation to extreme climate and basic state variation challenges a moisture mode view. *Journal*
412 *of Climate*, JCLI-D–15–0790.1, doi:10.1175/JCLI-D-15-0790.1, URL [http://journals.ametsoc.](http://journals.ametsoc.org/doi/abs/10.1175/JCLI-D-15-0790.1)
413 [org/doi/abs/10.1175/JCLI-D-15-0790.1](http://journals.ametsoc.org/doi/abs/10.1175/JCLI-D-15-0790.1).

414 Seidel, S., and D. Yang, 2018: The virtual effect of water vapor helps stabilize tropical climate.
415 *AGU Fall Meeting*, URL <https://agu.confex.com/agu/fm18/meetingapp.cgi/Paper/423217>.

416 Sobel, A. H., J. Nilsson, and L. M. Polvani, 2001: The Weak Temperature Gradient Approximation
417 and Balanced Tropical Moisture Waves*. *Journal of the Atmospheric Sciences*, **58** (23), 3650–
418 3665, doi:10.1175/1520-0469(2001)058<3650:TWTGAA>2.0.CO;2.

419 Tompkins, A. M., 2001: Organization of Tropical Convection in Low Vertical Wind Shears:
420 The Role of Water Vapor. *Journal of the Atmospheric Sciences*, **58** (6), 529–545, doi:
421 10.1175/1520-0469(2001)058<0529:OOTCIL>2.0.CO;2, URL [http://journals.ametsoc.org/doi/](http://journals.ametsoc.org/doi/abs/10.1175/1520-0469(2001)058{\%}3C0529:OOTCIL{\%}3E2.0.CO;2)
422 [abs/10.1175/1520-0469\(2001\)058{\%}3C0529:OOTCIL{\%}3E2.0.CO;2](http://journals.ametsoc.org/doi/abs/10.1175/1520-0469(2001)058{\%}3C0529:OOTCIL{\%}3E2.0.CO;2).

423 Yang, D., 2018a: Boundary layer diabatic processes, the virtual effect, and convective
424 self-aggregation. *Journal of Advances in Modeling Earth Systems*, **10** (9), 2163–2176,
425 doi:10.1029/2017MS001261, URL [https://agupubs.onlinelibrary.wiley.com/doi/abs/10.1029/](https://agupubs.onlinelibrary.wiley.com/doi/abs/10.1029/2017MS001261)
426 [2017MS001261](https://agupubs.onlinelibrary.wiley.com/doi/pdf/10.1029/2017MS001261), <https://agupubs.onlinelibrary.wiley.com/doi/pdf/10.1029/2017MS001261>.

427 Yang, D., 2018b: Boundary layer height and buoyancy determine the horizontal scale of
428 convective self-aggregation. *Journal of the Atmospheric Sciences*, **75** (2), 469–478, doi:
429 10.1175/JAS-D-17-0150.1, URL <https://doi.org/10.1175/JAS-D-17-0150.1>, <https://doi.org/10.1175/JAS-D-17-0150.1>.

431 Yang, D., and A. P. Ingersoll, 2013: Triggered Convection, Gravity Waves, and the MJO: A
432 Shallow-Water Model. *Journal of the Atmospheric Sciences*, **70** (8), 2476–2486, doi:10.1175/
433 JAS-D-12-0255.1, URL <http://dx.doi.org/10.1175/JAS-D-12-0255.1>.

434 Yang, D., and A. P. Ingersoll, 2014: A theory of the MJO horizontal scale. *Geophysical Re-*
435 *search Letters*, 661–666, doi:10.1002/2013GL058542, URL [http://onlinelibrary.wiley.com/doi/](http://onlinelibrary.wiley.com/doi/10.1002/2013GL058542/epdf)
436 [10.1002/2013GL058542/epdf](http://onlinelibrary.wiley.com/doi/10.1002/2013GL058542/epdf).

437 Yang, J., and D. S. Abbot, 2014: A LOW-ORDER MODEL OF WATER VAPOR, CLOUDS,
438 AND THERMAL EMISSION FOR TIDALLY LOCKED TERRESTRIAL PLANETS. *The*
439 *Astrophysical Journal*, **784** (2), 155, doi:10.1088/0004-637x/784/2/155, URL [https://doi.org/](https://doi.org/10.1088/0004-637x/784/2/155)
440 [10.1088/0004-637x/784/2/155](https://doi.org/10.1088/0004-637x/784/2/155).

441 Yang, J., N. B. Cowan, and D. S. Abbot, 2013: STABILIZING CLOUD FEEDBACK DRAMAT-
442 ICALLY EXPANDS THE HABITABLE ZONE OF TIDALLY LOCKED PLANETS. *The As-*
443 *trophysical Journal*, **771** (2), L45, doi:10.1088/2041-8205/771/2/L45, URL <https://doi.org/10.1088/2041-8205/771/2/L45>,
444 [10.1088/2041-8205/771/2/L45](https://doi.org/10.1088/2041-8205/771/2/L45).

445 **LIST OF FIGURES**

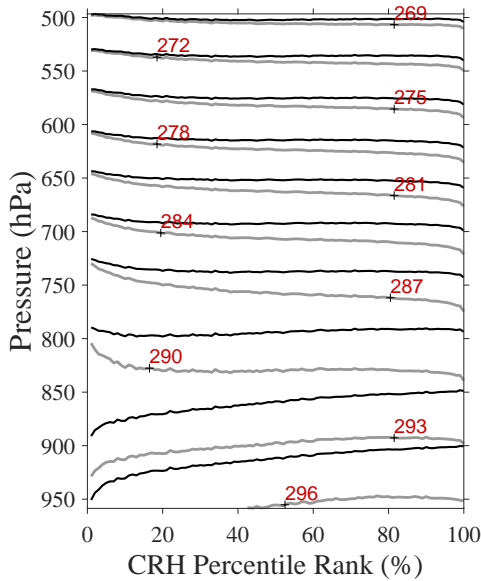
446 **Fig. 1.** Temperature and virtual temperature fields in the moisture space using NASA AIRS data
447 from 2°S to 2°N for the calendar year 2017. Black contours correspond to virtual tempera-
448 ture, and gray contours correspond to temperature. The x -axis is column relative humidity
449 (CRH) rank, where CRH was calculated as precipitable water divided by saturation precip-
450 itable water above the altitude of 850 hPa. The driest columns are to the left, and the moistest
451 columns are to the right. The temperature contours deviate from virtual temperature con-
452 tours due to the vapor buoyancy. In the free troposphere, the horizontal buoyancy gradient
453 is weak. Therefore, virtual temperature contours are approximately flat and temperature
454 increases toward dry columns. In the planetary boundary layer, surface drag can sustain sig-
455 nificant pressure gradients, and thereby buoyancy gradients. There, both virtual temperature
456 and temperature increase toward the moist column, forming a low pressure center over the
457 up-welling branch of the atmospheric circulation. 24

458 **Fig. 2.** Schematic diagrams. **a)** The vapor buoyancy effect increases OLR in the tropical atmo-
459 sphere. This figure depicts two stand-alone atmospheres: the control atmosphere (left);
460 no-vapor-buoyancy atmosphere (right). The horizontal axis is x or CRH; the vertical axis
461 is height (h = boundary layer height, H = tropopause height). The gray lines represent
462 temperature contours, and the black line represent buoyancy or virtual temperature contour.
463 The orange arrows represent OLR emission: large (small) arrow corresponds to more (less)
464 OLR. **b)** The negative climate feedback. Orange arrows represent an increase effect; the
465 blue arrow represents a decrease effect. 25

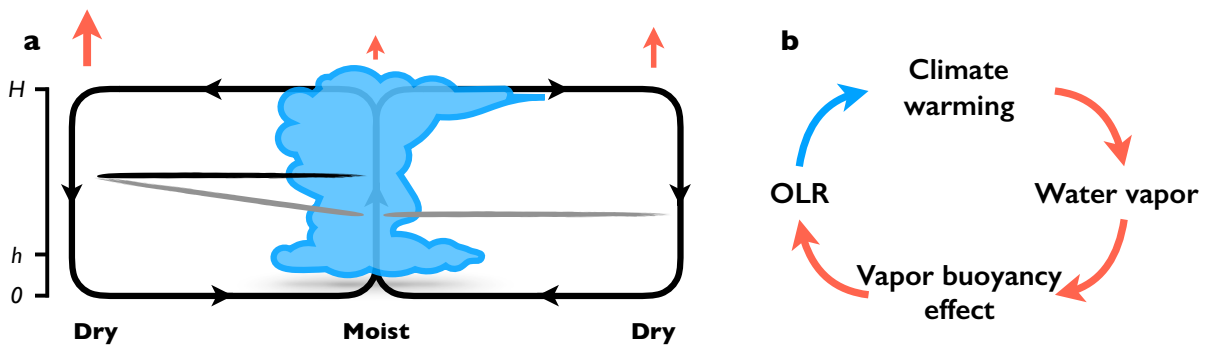
466 **Fig. 3.** (a) ΔT profiles (K). (b) τ profiles for the strong absorption band. (c) τ profiles for the weak
467 absorption band. Blue: 280 K, red: 300 K, yellow: 320 K. Dot-dashed: $\beta = 0.2$; solid:
468 $\beta = 0.5$; dashed: $\beta = 0.8$ 26

469 **Fig. 4.** (a) The radiative effect ΔOLR (W/m^2) due to the vapor buoyancy effect. The blue curve
470 corresponds to $\Delta OLR = 1 W/m^2$. (b) The total feedback parameter λ_t ($W/m^2/K$). (c) The
471 feedback parameter λ_{vb} ($W/m^2/K$) of the vapor buoyancy feedback. The blue curve cor-
472 responds to $\lambda = 0.1 W/m^2/K$ in (b-c). (d-f) ΔOLR , λ_t , and λ_{vb} for the free troposphere
473 ($p < 900$ hPa), respectively. 27

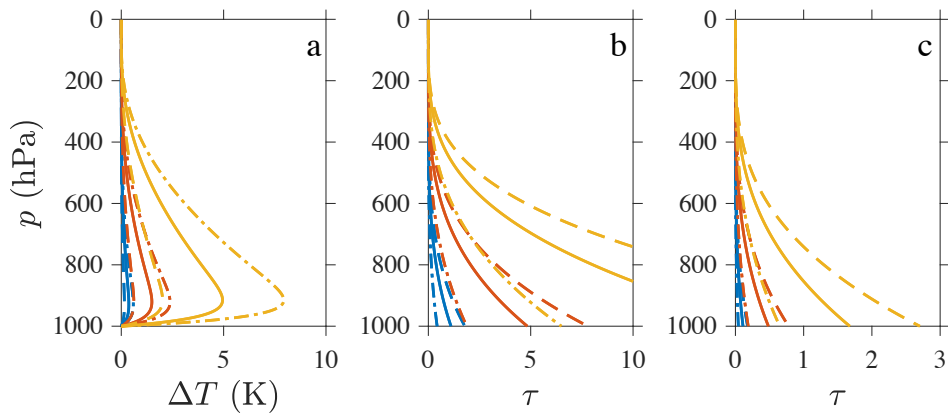
474 **Fig. 5.** Time-averaged temperature and moisture profiles at the Nauru ARM site during the period
475 from April 2001 to August 2013. (a) Specific humidity. (b) Relative humidity. (c) Tempera-
476 ture profiles. The red curve corresponds to the observed temperature profile; the blue curve
477 corresponds to the derived temperature profile of a convecting column. (d) Temperature dif-
478 ference, which is defined as red minus blue. Here we define the boundary layer top as 900
479 hPa, consistent with the definition in the simple model. 28



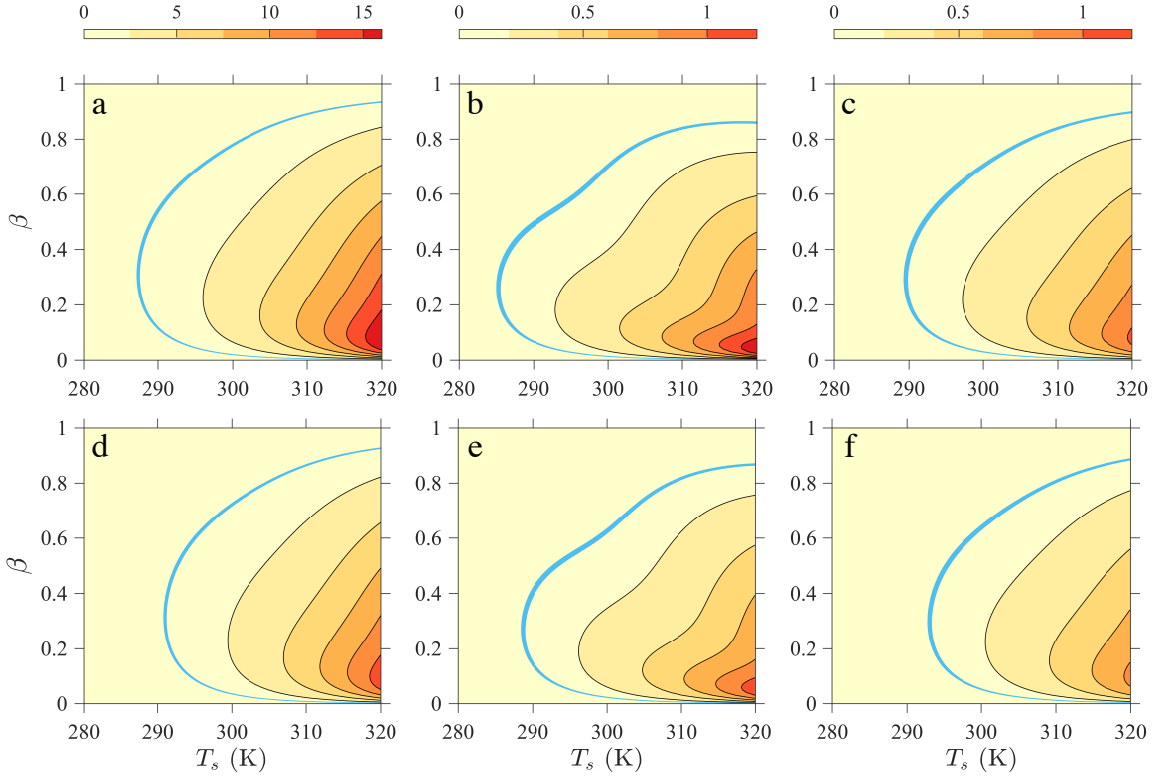
480 FIG. 1. Temperature and virtual temperature fields in the moisture space using NASA AIRS data from 2°S to
 481 2°N for the calendar year 2017. Black contours correspond to virtual temperature, and gray contours correspond
 482 to temperature. The x -axis is column relative humidity (CRH) rank, where CRH was calculated as precipitable
 483 water divided by saturation precipitable water above the altitude of 850 hPa. The driest columns are to the left,
 484 and the moistest columns are to the right. The temperature contours deviate from virtual temperature contours
 485 due to the vapor buoyancy. In the free troposphere, the horizontal buoyancy gradient is weak. Therefore, virtual
 486 temperature contours are approximately flat and temperature increases toward dry columns. In the planetary
 487 boundary layer, surface drag can sustain significant pressure gradients, and thereby buoyancy gradients. There,
 488 both virtual temperature and temperature increase toward the moist column, forming a low pressure center over
 489 the up-welling branch of the atmospheric circulation.



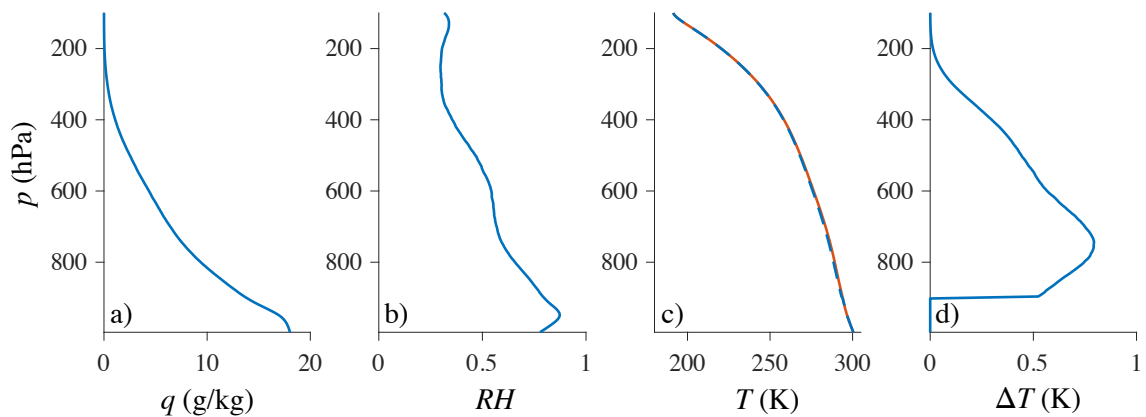
490 FIG. 2. Schematic diagrams. **a**) The vapor buoyancy effect increases OLR in the tropical atmosphere. This fig-
 491 ure depicts two stand-alone atmospheres: the control atmosphere (left); no-vapor-buoyancy atmosphere (right).
 492 The horizontal axis is x or CRH; the vertical axis is height (h = boundary layer height, H = tropopause height).
 493 The gray lines represent temperature contours, and the black line represent buoyancy or virtual temperature
 494 contour. The orange arrows represent OLR emission: large (small) arrow corresponds to more (less) OLR. **b**)
 495 The negative climate feedback. Orange arrows represent an increase effect; the blue arrow represents a decrease
 496 effect.



497 FIG. 3. (a) ΔT profiles (K). (b) τ profiles for the strong absorption band. (c) τ profiles for the weak absorption
 498 band. Blue: 280 K, red: 300 K, yellow: 320 K. Dot-dashed: $\beta = 0.2$; solid: $\beta = 0.5$; dashed: $\beta = 0.8$.



499 FIG. 4. (a) The radiative effect ΔOLR (W/m^2) due to the vapor buoyancy effect. The blue curve corresponds
 500 to $\Delta OLR = 1 \text{ W}/\text{m}^2$. (b) The total feedback parameter λ_t ($\text{W}/\text{m}^2/\text{K}$). (c) The feedback parameter λ_{vb} ($\text{W}/\text{m}^2/\text{K}$)
 501 of the vapor buoyancy feedback. The blue curve corresponds to $\lambda = 0.1 \text{ W}/\text{m}^2/\text{K}$ in (b-c). (d-f) ΔOLR , λ_t , and
 502 λ_{vb} for the free troposphere ($p < 900 \text{ hPa}$), respectively.



503 FIG. 5. Time-averaged temperature and moisture profiles at the Nauru ARM site during the period from April
 504 2001 to August 2013. (a) Specific humidity. (b) Relative humidity. (c) Temperature profiles. The red curve
 505 corresponds to the observed temperature profile; the blue curve corresponds to the derived temperature profile
 506 of a convecting column. (d) Temperature difference, which is defined as red minus blue. Here we define the
 507 boundary layer top as 900 hPa, consistent with the definition in the simple model.